Probing the RGB-phase transition: Near–IR photometry of six intermediate age LMC clusters

Francesco R. Ferraro

Dipartimento di Astronomia, Università degli Studi di Bologna, Via Ranzani, 1 - 40127 Bologna, ITALY

ferraro@bo.astro.it

Livia Origlia

INAF - Osservatorio Astronomico di Bologna, Via Ranzani, 1 - 40127 Bologna, ITALY

origlia@bo.astro.it

Vincenzo Testa

INAF - Osservatorio Astronomico di Roma, Via Frascati, 33 - 00040 Monteporzio Catone, ITALY

testa@mporzio.astro.it

and

Claudia Maraston

Max-Planck-Institut für Extraterrestrische Physik, Giessenbachstrae, 85748 Garching bei München, GERMANY

maraston@mpe.mpg.de

ABSTRACT

This is the first of a series of papers devoted to a global study of the photometric properties of the red stellar sequences in a complete sample of the Large Magellanic Cloud clusters, by means of near infrared array photometry. Deep J,H,Ks photometry and accurate Color Magnitude Diagrams down to K $\approx$ 18.5,

[1]Based on observations collected at the European Southern Observatory, La Silla, Chile, using SOFI at the 3.5m NTT, within the observing programs 64.N-0038 and 68.D-0287.

i.e. ≈ 1.5 mag below the red He-clump, for six intermediate age clusters (namely NGC 1987, NGC 2108, NGC 2190, NGC 2209, NGC 2231, NGC 2249) are presented. A quantitative estimate of the population ratios (by number and luminosity) between Red Giant Branch and He-clump stars for each target cluster is provided and discussed in the framework of probing the so-called Red Giant Branch phase transition (RGB *Ph-T*). By using the Elson & Fall *s-parameter* as an age indicator, the observed RGB population shows a sharp enhancement (both in number and luminosity) at $s = 36$. Obviously, the corresponding absolute age strictly depends on the details of theoretical models adopted to calibrate the *s*-parameter. Curiously, the currently available calibrations of the *s*-parameter in term of age based on *canonical* (by Elson & Fall 1988) and *overshooting* (Girardi et al. 1995) models provide ages that well agree within 10%, suggesting that the full development of the Red Giant Branch occurs at $t \approx 700$ Myr and be a relatively fast event ($\delta t \approx 300$ Myr).
However, the RGB *Ph-T* epoch derived from the *overshooting* calibration of the *s*-parameter turns out to be significantly earlier than the epoch provided by the recent evolutionary tracks by Girardi et al. (2000). A new calibration of the *s*-parameter based on high quality Color Magnitude Diagrams and updated models is urged to address the origin of this discrepancy and finally establish the epoch of the RGB *Ph-T*.

Subject headings: Magellanic Clouds, globular clusters: individual (NGC 1987, NGC 2108, NGC 2190, NGC 2209, NGC 2231, NGC 2249), techniques: photometric, infrared: stars

1. Introduction

Stellar evolution theory predicts that evolved red giant stars dominate the bolometric luminosity of a Simple Stellar Population (SSP) after a few hundred million years. Theoretical models (Renzini & Buzzoni 1986; Bruzual & Charlot 1993; Maraston 1998) suggest that two special events (the so–called *Phase Transitions, Ph–T*) significantly mark the spectral evolution of a SSP during its lifetime. The first, after $\approx 10^8$ yrs, due to the sudden appearance of red and bright Asymptotic Giant Branch (AGB) stars (AGB *Ph–T*), and the second, after $\approx 6 \times 10^8$ yrs, due to the development of the full Red Giant Branch (RGB *Ph–T*).

From an observational point of view, the globular cluster system of the Magellanic Clouds (MC) provides an unique opportunity to study the AGB and RGB properties (morphology, luminosity function etc.) with varying the age and chemical composition of the

stellar population. It has been known for a long time that MC clusters are different in many respect from those in the Milky Way. They represent the *ideal laboratory* to investigate the spectral behavior of a SSP since they cover a wide range in age (see e.g. Searle, Wilkinson, & Bagnuolo 1980; Elson & Fall 1985; Girardi et al. 1995), and metallicity (see e.g. Sagar & Pandey 1989). They also have a wide spread in integrated colors: Persson et al. (1983) showed that very young blue clusters (SWB–type I–III) do not have extended AGB or RGB sequences, while red clusters having SWB–type V or later display a well populated AGB and RGB. Hence, SWB–type IV clusters represent the transition class which starts to populate the giant branches of the Color Magnitude Diagram (CMD) and whose integrated colors become red (see also Fig.1 in Ferraro et al. 1995, hereafter F95).

In the last decade high quality optical CMDs of MC cluster from both ground-based (see e.g. Brocato et al. 1996; Testa et al. 1999; Dirsch et al. 2000) and HST (see e.g. Olsen et al. 1998; Brocato, Di Carlo & Menna 2001; Rich, Shara & Zurek 2001; Matteucci et al. 2002) observations down to the Turn-off have been obtained.

However, such an optical photometric database need to be complemented with high quality and homogeneous IR photometry, to properly study the red stellar sequences. In this respect, we have undergoing a long-term project devoted to study the photometric properties of the AGB and RGB with varying the stellar age and metallicity in the stellar clusters of our Galaxy and in the MC, by coupling the information from optical and near IR CMDs and Luminosity Functions (LFs) (Ferraro et al. 1999, 2000).

Near IR observations are crucial in such a study since they provide the highest sensitivity to the physical parameters of cool stars and the contrast between red giants and the unresolved background is greater than in any other spectral range. This drastically reduces the crowding effects in the innermost regions of the clusters and it also represents a major, conceptual simplification in the interpretation of the integrated spectrum.

A preliminary IR survey of 12 intermediate age LMC clusters has been performed at the CTIO with the first generation IRIM (58×64 pixel) imager (see F95). Although the large pixel size and the moderate performance of the detector strongly limited the quality of the photometry in the crowded central region, we sampled a good number of giants along the bright portion (i.e. $14.3 < K < 12.3$) of the RGB sequence (see Figures 5a,b in F95). This dataset was successfully used to derive the first direct observational evidence of the RGB *Ph–T* (see F95 for a full discussion). However, the limited extension in magnitude of the sample prevented us to quantify the global contribution of the RGB to the integrated cluster bolometric light and to perform a detailed comparison with the theoretical expectations (see Fig. 23 in Maraston 1998).

More recently, taking advantage of the superior performances of the new generation of 1024×1024 IR array detectors available at the ESO telescopes, we performed a photometric survey of a complete sample of LMC clusters of different ages. Homogeneous J,H,Ks photometry 1.5 magnitude below the He-clump have been obtained for 20 clusters (spanning an age range between 10^8 and a few 10^9 yrs) during two successful observational runs.

This is the first of a series of papers devoted to study the photometric properties of the observed clusters. In this paper, we present the results from the first run of observations in which near IR photometry of 6 LMC clusters with intermediate-age has been secured. This sample represents $\approx 30\%$ of the global dataset secured within this project.

2. Observations and photometric analysis

J,H,Ks images of six intermediate age globular clusters in the LMC (cf. Table 1) have been obtained at ESO, La Silla, on January 12-14, 2000, by using the near IR imager/-spectrometer SOFI (Moorwood, Cuby & Lidman 1998) mounted at the ESO 3.5m NTT. SOFI is an imager/spectrometer equipped with a 1024×1024 Rockwell IR-array detector; in the imaging mode the camera can be used with two different pixel scales: $0.292''/pixel$ and $0.145''/pixel$. All the observations presented here, have been performed with a scale of $0.292''/pixel$, providing a $\approx 5' \times 5'$ field of view each frame. Total integration times of 2 min in J,H and 8 min in Ks split into sets of shorter exposures have been achieved, allowing photometry down to J$\approx$19 and H,Ks$\approx$18.5 with a S/N$\geq$30.

A control field a few arcmin away from each cluster center has been also observed using the same instrumental configuration, in order to construct median-averaged sky frames. A large sample of high S/N flatfields in each filter have been acquired by using an halogen lamp, alternatively switch on and off. The final cluster and control field frames are sky–subtracted and flatfield corrected. For each cluster, the dataset includes three J,H,Ks images, centered on the cluster and three corresponding frames of an external field.

The photometric analysis was done by using *daophot-II* under IRAF. For each observed field all the images in the J,H,Ks filters were carefully aligned and trimmed in order to have three output images, one per filter, slightly smaller than the original ones but perfectly registered. Then, a first *daophot-II* Point Spread function (PSF) fitting run was applied to the J image. The output catalog with the instrumental magnitudes has been checked for any spurious detection or missing object (typically 3–4 stars at most) which have been included in the catalog by hand. The J catalog was then used as input *master* list to perform PSF fitting on the H and Ks images.

A set of seven photometric standard stars spanning a wide range of (J−K) colors (about two magnitudes) from the list of Persson et al. (1998) have been observed during each night. Each standard star was observed in a sequence of five measurements per filter in different positions on the array. As usual, aperture photometry has been applied to each single frame and multiple measurements in each filter for each standard star have been averaged together. The final calibration of the run linking the instrumental aperture photometry (*daophot-II* output) with the photometric standard system are as follows (see also Figure 1):

$$\mathrm{K} - \mathrm{ks} = -2.396 \pm 0.019$$

$$\mathrm{H} - \mathrm{h} = -1.795 \pm 0.019$$

$$\mathrm{J} - \mathrm{j} = -1.694 \pm 0.022$$

where j, h, ks are instrumental aperture magnitude, normalized at $t_{exp} = 1sec$ and J,H,K are the corresponding magnitudes from the list of Persson et al. (1998). Observations have been performed in the Ks filter but the calibration has been reported to the standard K filter. From the inspection of Figure 1 it is clear that the color term (if any) is very small and it can be neglected.

As usual, the most isolated brightest stars in each science field have been used to link the aperture magnitudes to the instrumental ones as obtained from the PSF-fitting procedure. The calibrated photometric catalogs in each filter were finally matched and merged together in a global catalog. The final database consists of a table per cluster, listing positions and magnitudes for all the detected objects. Table 2 shows an extract of the whole database, which is entirely available in electronic form.

3. Color–Magnitude and Color–Color Diagrams

Figures 2 and 3 show the CMDs for the observed clusters in the (K, J−K) and (H, J−H) planes, respectively. All stars with $r < 1.5'$ from the cluster center (evaluated by eye directly on the image) have been plotted. This selection has been done in order to minimize the field contamination and to allow a fist-order inspection of the cluster population.

Figure 4 shows the (K, J − K) CMDs for the external regions (at $r > 2'$ from the cluster center) of the six clusters. These diagrams can be considered representative of the field population. From the comparison of Figures 2 and 4, taking into account that the field refer to an area which is double in size with respect to the one sampled by the *contaminated* cluster population, one can see that only two clusters in our sample, namely NGC 1987 and NGC 2108, show significant field contamination.

The main characteristics of the CMDs can be schematically summarized as follows:

(i) Magnitude limits down to H,K$\approx$ 18.5, i.e. about 1.5 mag below the He-clump, which is clearly visible as a concentration of stars at K $\approx$ 17.

(ii) The brightest objects at K $<$ 12 are more likely AGB stars.

(iii) The RGB appears as a well-populated sequence at K $>$ 14 in three clusters, namely NGC 1987, NGC 2108 and NGC 2231, although a significant fraction of stars in NGC 1987 and NGC 2108 can belong to the field population. At K $\lesssim$ 14 very few giants are observed.

(iv) In the other three clusters, namely NGC 2190, NGC 2209 and NGC 2249 only the red He-clump region at K $\approx$ 17 is well-populated, while the upper RGB is barely defined.

According to the historical Searle, Wilkinson, & Bagnuolo (1980) classification based on the *s*-parameter and subsequent calibrations of such a parameter with age (see e.g. Elson & Fall 1985; Girardi et al. 1995), the LMC clusters in our sample should have ages in the 500-900 Myr range (see Table 1 and Section 5.4) and are expected to be on the verge of the RGB *Ph–T* (see also F95).

In order to perform a quantitative analysis of the population distribution along the evolved sequences and to compare the results with theoretical predictions, we construct de-reddened CMDs and select suitable regions to define the AGB and RGB populations.

Correction for extinction is computed according to the E(B$-$V) values reported in Table 1 and the Rieke & Lebofsky (1985) interstellar extinction law. The infrared dust maps by Schlegel, Finkbeiner, & Davis (1998) in the direction of the observed clusters provide very similar (on average within $\pm$0.03 dex) E(B$-$V) corrections, with the exception of NGC 2108, for which the discrepancy is about 0.1 dex. However, the overall impact of such a discrepancy on the infrared magnitudes is always small (well within 0.1 dex), hence reddening correction is not a critical issue in this context.

Figure 5 shows the cumulative $K_0, (J-K)_0$ CMD for the six observed clusters. On this CMD we identified three *selection boxes* sampling the bulk of the AGB, RGB and He-clump populations, respectively (see Figure 5). According to the observed near IR CMDs of the 10 LMC clusters by F95, the RGB Tip is expected to be at $K_0 \approx 12.3$. Recently, this value has been confirmed by computing the RGB LF of the LMC field population from the 2MASS survey (Nikolaev & Weinberg 2000). From the DENIS survey Cioni et al. (2000) defined a slightly brighter (by $\approx$0.2 mag) RGB Tip than F95 and Nikolaev & Weinberg (2000). However, since small differences in the location of the RGB Tip have negligible effects on our analysis we do not consider this issue crucial and we adopted the F95 and Nikolaev & Weinberg (2000) value. Stars brighter than the RGB Tip at $K_0 \approx 12.3$ and with

$(J-K)_0$ colors between 0.85 and 2.1 are thus classified as AGB. The bulk of the bright RGB population includes all the stars ≈4 mag from the RGB Tip down to $K_0 \approx 16.3$ with $(J-K)_0$ colors between 0.32 and 1.21 (see Figure 5). The faint end of the RGB *selection box* has been conservatively assumed at $K_0 = 16.3$ (i.e. ≈ 0.7 mag brighter than the He-clump peak at $K_0 = 17.0$), in order to avoid a possible contamination by the He-clump distribution wings (which are extending up to ±0.5 mag from the peak, see right panel of Figure 5).

Figure 6 shows the cumulative $(J-H)_0, (H-K)_0$ de-reddened color–color diagram for the six observed LMC clusters. The majority of the brightest stars at $K_0 < 12.3$ have very red $(J-H)_0$ and $(H-K)_0$ colors, typical of long period variables and/or carbon stars which are the brightest extension of the AGB evolutionary stage, usually significantly brighter that the RGB-Tip. This is a further confirmation that our RGB Tip assumption ($K_0 \approx 12.3$) is correct.

4. Star counts and integrated luminosities

In each cluster the observed stars have been classified as AGB, RGB and He-clump stars, accordingly to the *selection boxes* defined in Section 3 and sketched in Figure 5.

In order to obtain reliable stellar counts and integrated luminosities in each evolutionary sequence, it is also necessary to estimate the degree of completeness of the sample and its possible contamination by the foreground/background stars and to correct for them.

4.1. Completeness

Completeness has been estimated by using the well known artificial star techniques. Here, we briefly recall the main steps. The RGB fiducial line for each cluster was derived, then a population of artificial stars, having magnitudes, colors and luminosity function resembling those of the observed RGB distribution was generated and added to the original images. Only a sub-raster centered on the cluster and included within a radius of 1'.5×1'.5 was used to estimate completeness. Outside this area crowding effects are negligible and the completeness level is ≈ 100%.

A total of 100,000 stars were simulated with a distribution resembling the observed one. The fraction of recovered objects was estimated as $\Lambda = N_{rec}/N_{sim}$. The observed distribution is in principle distorted because of two phenomena: the loss of faint stars due to incompleteness and an excess of bright stars due to possible blending of two or more faint stars into a brighter one. The first effect is taken into account by the artificial star simulation.

The second is more complicated and it can be evaluated by analyzing the histogram of the magnitude difference between input and recovered magnitudes. It turns to be negligible (see also discussion in Testa et al. 1999, and references therein).

Figure 7 shows the curves of completeness for the target clusters in two different annuli, namely r$\leq$18" and r>18" within the selected 1.5'×1.5' area. At K $<$ 14 completeness is always >95%. At K $\approx$ 17 completeness is $\geq$80% in the outer annulus and $\geq$50% in the inner one where crowding is more severe. The cutoff radius which divides the two annuli was set on the basis of the radial stellar distribution. However, its choice is not critical since reasonable small variations (within $\approx$20%) from our best-fiducial value turns out to have negligible effects on the results.

4.2. Field de-contamination

The issue of de-contaminating the observed star distribution from the field contribution is rather tricky. The method usually employed is known as *zapping technique*: the CMDs of the *contaminated* cluster and the field populations are divided in cells of fixed magnitude and color widths. After normalizing the areas, the *cleaned* CMD is obtained by randomly subtracting, cell by cell, the number of stars found in the field CMD from the *contaminated* cluster one. This technique has some drawbacks which are described in detail in various papers (see e.g. the discussion in Testa et al. 1999, and references therein). In our case, the main limitation is the relatively low number statistics of some cells, which can generate a *cleaned* CMD with a patchy distribution and entire zones artificially de-populated.

We thus preferred to directly de-contaminate the star counts. The stars in the inner region (within a radius of 1.5' from the cluster center) are considered as representative of the cluster *contaminated* population, while those in the outermost regions (at a radius of $\gtrsim 2'$ from the cluster center) as representative of the field population.

The total number of stars observed in each evolutionary sequence (AGB, RGB and He-clump) has been counted accordingly to the *selection boxes* shown in Figure 5 both in the *contaminated* cluster and field CMDs. The star counts from the *contaminated* cluster population have been then corrected for incompleteness adopting the curves shown in Figure 7. The star counts in the field population have been scaled to take into account the different surveyed area, and their contribution has been subtracted from the cluster *contaminated* population. At the end of this procedure *cleaned* LFs for each evolutionary sequence and in each cluster have been finally obtained.

Table 3 list the final star counts in each sequence for the de-contaminated cluster and

field populations. As already mentioned, two clusters in our sample, namely NGC 1987 and NGC 2108, have a significant degree of field contamination, ≈46 and 41% by number, respectively. For the other clusters the degree of field contamination is much lower (between 10 and 24%).

5. Population ratios and evolutionary timescales

When dealing with resolved stellar populations a number of interesting tests of theoretical models of stellar evolution can be performed. In this respect, population ratios (by numbers and/or by luminosity) are crucial tools to calibrate the relative lifetimes (and luminosity contribution) of each specific evolutionary sequence, to identify special events like the *phase transitions*, and to check the overall reliability of the stellar clock.

5.1. Definition of the observables

As mentioned in Section 1, F95 presented preliminary observational evidences that the RGB *Ph–T* does occur at $s = 35 - 36$, however due to the modest performances of the IR detector used at that time the analysis was limited to the brightest 2-mag bin of the RGB ($12.3 < \mathrm{K}_0 < 14.3$). In order to account for the size of the total cluster population, both star counts and luminosity of the upper RGB in F95 were normalized to the cluster integrated luminosity (in unit of $10^4 L_\odot$ taken from Persson et al. 1983). The adopted normalization was the only possible one, due to the limited extension in magnitude of the CMD. However, it should be noted that the integrated luminosity of intermediate-age clusters can be easily dominated by the few bright AGB stars, hence it can be significantly affected by stochastic effects due to the intrinsic low number statistics characterizing the AGB evolutionary phase (Chiosi et al. 1986; Santos & Frogel 1997, see also Figure 11 in F95).

An alternative *full empirical* normalization, less affected by stochastic effects, can be obtained by using the He-clump population. All the intermediate-age and old stars are indeed expected to experience a stable He core-burning phase (see e.g. Olszewski, Suntzeff & Mateo 1996, for a review), whose signature in the CMD is a red clump about $\delta\mathrm{K} \approx 5$ mag below the RGB Tip. The He-clump is clearly visible in all the CMDs shown in Figures 2 and 3, hence two observables (which can be directly estimated from the CMD) can be defined: the population ratio between the RGB and He-clump (N_{RGB}/N_{He-C}) number of stars and their corresponding luminosities ($L^{bol}_{RGB}/L^{bol}_{He-C}$).

Global luminosities for each evolutionary stage have been computed by summing the

contribution of the single stars in the completeness-corrected and field de-contaminated LF obtained for each *selection box* defined in Section 3 and in Figure 5. In particular, the de-reddened K-band magnitudes have been scaled to absolute values by adopting a distance modulus $(m - M)_0 = 18.5$ (van den Berg 1998; Nikolaev & Weinberg 2000) and converted to bolometric magnitudes by applying suitable bolometric corrections (as derived by using the $(J - K)_0$ color and the empirical calibrations by Montegriffo et al. (1998). The derived *integrated* bolometric luminosities (in unit of $10^4 L_\odot$) for each evolutionary stage (AGB, RGB,i He-clump) are listed in Table 3.

5.2. Theoretical models

Theoretical predictions for the observables defined in the previous section have been computed by using SSP models by Maraston (1998) and Maraston et al. (2001), for which the synthetic colors have been calibrated on the observed integrated colors of MC clusters.

The adopted evolutionary code estimates the energetics of any post-MS phase by using the so-called *Fuel Consumption Theorem* (Renzini & Buzzoni 1986) and allows to model the two key AGB and RGB *phase transitions*.

The main synthetic ingredients which mostly influence the theoretical predictions are:

(i) the adopted stellar evolutionary tracks. The stellar tracks used here are taken from Cassisi & Salaris (1997); Bono et al. (1997). These are *canonical* tracks, without *overshooting*, in which the most recent input physics (opacities, equation of state, etc.) are adopted. The mixing-length parameter has been calibrated on the Sun and scaled to other metallicities by using empirical relations (Salaris & Cassisi 1996).

(ii) the integration method. The method adopted to determine the number of stars (and luminosity) in any post-MS phase in the *Fuel Consumption* approach is different with respect to that used in the isochrone technique, which is based on the mass dispersion along the post-MS phases. Conversely here, the post-MS stellar track of a mass equal to the Turnoff mass at a given stellar population age is divided into a suitable number of sub-phases. Then, the evolutionary timescale is combined with the Fuel Consumption in order to evaluate the number of stars and their luminosity in each sub-phase (Maraston 1998; Maraston et al. 2001, more details can be found in).

(iii) the temperature-color transformations. Transformations are taken from the BaSel tables (Lejeune et al. 1997), in which the classical Kurucz library down to 3500 K is linked to models for cooler temperatures (Bessel et al. 1998), and re-calibrated on observed colors

of individual stars.

In order to make a preliminary check of the impact of the different treatment of mixing on the observables described in Section 5.1, we have computed SSP models with the procedure outlined in this section, but adopting the stellar tracks with *overshooting* from Girardi et al. (2000). We have chosen these tracks among the several including a parameterization of overshooting, since in F95 we used an earlier release of the Padova tracks. In a future work we will explore other sets of stellar tracks that do include an overshooting effect, but with different efficiency (see e.g. Yi et al. (2001)). Indeed, as quoted by Gallart et al. (2003) the extension and efficiency of overshooting is still not well established, and the comparison with observations is crucial.

5.3. Age calibration

Since in the literature an homogeneous set of age determinations based on the MS-TO is still lacking for MC clusters, we have used the so-called *s*-parameter. This parameter was defined by Elson & Fall (1985) as a curvilinear coordinate running along the mean locus defined by MC clusters in the $(U-B, B-V)$ integrated color-color diagram and it turns out to vary from 1 (very young clusters) to 51 (very old cluster).

Of course, the absolute age for the programme clusters obtained via the *s*-parameter strictly depends on the adopted calibration, which, in turn, depends on the details of the theoretical models of stellar evolution and, in particular, on the treatment of the convection. We adopted two different calibrations available in the literature:

1) the calibration obtained by Elson & Fall (1988, hereafter EF88) based on *canonical* models:

$$log\ t = 6.05 + 0.079 \times s$$

2) the *overshooting* calibration presented by Girardi et al. (1995) and based on the models with *overshooting* by Bertelli et al. (1994):

$$log\ t = 6.227 + 0.0733 \times s$$

Table 4 lists the ages of the six clusters in our sample as obtained from the *s*-parameter, using the two above calibrations (see column 3 and 4). Surprisingly, the two calibrations provide very similar ages (within 10%), hence in the following we adopt the most recent one by Girardi et al. (1995), finding that the target clusters span an age range between ≈500 and 900 Myr. Table 4 also lists the few age determinations available in the literature from direct measurements of the MS-TO. Ages determined through the *s*-parameter calibrations

agree with the TO ones within 20–30%. Hence one can safely conclude that the *s*-parameter provides a reasonable estimate (within $\pm \simeq$20%) of the cluster age. According with this result, a conservative estimate of the error ($\approx$ 20%) in the age determination has been assigned to each cluster, this value has been computed assuming an uncertainty of $\delta s = \pm 1$, which correspond to $\delta(age) = \pm 100$ Myr at $s = 35$ ($t \approx 620$ Myr).

5.4. Comparison between observations and model predictions

Figure 8 shows the ratio between the number of RGB and the He-clump stars in each cluster, according to the selection criteria illustrated in Section 3 and in Figure 5, as a function of the cluster age. Figure 9 shows the ratio between the corresponding bolometric luminosities. By inspection of Figure 8 and 9 one can see that the contribution of the RGB phase increases by a factor of $\approx$3 by number (cf. Figure 8 and Table 3) and $\approx$4 by luminosity (cf. Figure 9 and Table 3) in less than $\approx$ 400 Myr.

Both Figures 8 and 9 support the hypothesis that the cluster set presented here properly sample the epoch of the full development (both in luminosity and in star number) of the RGB. This result fully confirms the finding by F95 who identified NGC1987 and NGC2108 as the two intermediate-age clusters on the verge of the RGB *Ph–T*.

The lines in Figure 8 and 9 represent model predictions: short-dashed and solid lines, *canonical* models (Maraston 1998, see also Section 5.2), at two different metallicities, namely [Z/H]=–0.33 and –1.35, respectively, long-dashed line model with *overshooting* (Girardi et al. 2000) at [Z/H]=–0.4 and Y=0.25, the most representative for the LMC (see e.g. Girardi & Bertelli 1998).

The time-scale yielded by the two calibrations of the *s*-parameter discussed in Section 5.1 shows a nice agreement with that defined by the *canonical* models, suggesting that the RGB *Ph–T* occurs at $t \approx 700$ Myr and it is a quite rapid event since the main increase of the RGB luminosity occurs in less than $\delta t \approx 300$ Myr.

Both *overshooting* and *canonical* models agree with observations in showing that the RGB *Ph–T* is a rapid event ($\delta t \approx 300$ Myr). However, evolutionary tracks with *overshooting* predict the RGB *Ph–T* occurrence at significantly later ($\Delta t \simeq 500$ Myr) epochs than the one indicated by *canonical* models. Indeed, by carefully inspecting the Girardi et al. (2000) isochrones, one finds that at t=1 Gyr the RGB-tip luminosity is still steeply increasing: at $[M/H] = -0.4$ the absolute magnitude of the RGB-Tip ($M_V(RGB - tip)$) changes from $M_V(RGB - tip) = -0.71$ at t=1 Gyr to $M_V(RGB - tip) = -2$ at t=1.4 Gyr. This confirms that at the epoch ($t \approx 1$ Gyr) at which the RGB *Ph–T* is almost completed in the *canonical*

models (see Figure 8 and 9), it is still under development when using the *overshooting* evolutionary tracks.

The mismatch shown in Figures 8 and 9 suggest some problems with the evolutionary timescales of the *overshooting* models by Girardi et al. (2000) and/or with the Girardi et al. (1995) calibration of the *s*-parameter. However, a similar discrepancy was already noted by F95 in the previous generation of *overshooting* models.
A new calibration of the *s*-parameter in terms of age by using high quality CMDs and updated models is urgently needed to clarify this issue.

6. Summary and future work

In this paper we present the photometric analysis based on near IR CMDs down to K $\approx$ 18.5 of the six intermediate-age LMC clusters, namely NGC 1987, NGC 2108, NGC 2190, NGC 2209, NGC 2231 and NGC 2249, in our sample. More than 4,000 giant stars in the cluster and surrounding field populations have been studied.

As a suitable diagnostics to probe the existence of the RGB *Ph–T* we use the ratios (by number and luminosity) between the RGB and He-clump populations. Empirical estimates have been compared with model predictions. The observed RGB population shows a sharp enhancement (both in number and luminosity) at $s = 36$. This corresponds to $t \approx 700$ Myr, accordingly with the current available calibrations of the *s*-parameter (both using *canonical* and *overshooting* models). However, in the case of models with overshooting, a significant discrepancy between the timescale provided by the *s*-parameter and the one set by the evolutionary tracks has been found. The origin of such a discrepancy needs to be further investigated.

In forthcoming papers we will present the near IR CMDs for the other MC clusters in our sample, spanning the full age range between 10^8 and a few 10^9 yrs. The analysis of the entire sample will allow us to fully characterize the photometric properties of the AGB, RGB and He-clump sequences with varying the age of the stellar population.

The financial support by the Agenzia Spaziale Italiana (ASI) and the Ministero dell'Istruzione, Università e Ricerca (MIUR) is kindly acknowledged.

REFERENCES

Bertelli, G., Bressan, A., Chiosi, C., Fagotto, F., & Nasi, E., 1994, A&AS, 106, 275

Bessel, M. S., & Brett, J. M. 1988, PASP, 100, 1134

Bessel, M. S., Brett, J. M., Wood, P. R., Scholz, M., 1989, A&ASS, 77, 1

Bono, G., Caputo, F., Cassisi, S., Castellani, V., & Marconi M., 1997, ApJ, 479, 279

Bruzual, A. G., and Charlot, S. 1993, ApJ, 405, 538

Brocato, E., Castellani, V., Ferraro, F. R., Piersimoni, A. M., & Testa V. 1996, MNRAS, 282, 614

Brocato, E., Di Carlo, E., & Menna, G. 2001, A&A, 374, 523

Cassisi, S., & Salaris, M., MNRAS, 285, 593

Chiosi, C., Bertelli, G., Bressan, A., & Nasi, E., 1986, A&A, 165, 84

Cioni, M. R. L., van der Marel, R. P., Loup, C. & Habing, H. J. 2000, A&A, 359, 601

Corsi, C.E., Buonanno, R., Fusi Pecci, F., Ferraro, F.R., Testa, V., & Greggio, L., 1994, MNRAS, 271, 385

Dirssch, B., Richtler, T., Gieren, W. P., & Hiller, M. 2000, A&A, 360, 133

Elson, R. A., & Fall, S. M. 1985, ApJ, 299, 211

Elson, R. A., & Fall, S. M. 1988, AJ, 96, 1383 (EF88)

Ferraro, F. R., Fusi Pecci, F., Testa, V., Greggio, L., Corsi, C. E., Buonanno, R., Terndrup, D. M., & Zinnecker, H. 1995, MNRAS, 272, 391 (F95)

Ferraro, F. R., Messineo, M., Fusi Pecci, F., de Palo, M. A., Straniero, O., Chieffi, A., & Limongi, M. 1999, AJ, 118, 1738

Ferraro, F. R., Montegriffo, P., Origlia, L., & Fusi Pecci, F. 2000, AJ, 119, 1282

Frogel, J.A., Persson, S.E., Aaronson, M., Matthews, K., 1978, ApJ, 272, 488

Gallart, C., Zoccali, M., Bertelli, G., Chiosi, C., Demarque, P., Girardi, L., Nasi, E., Woo, J., & Yi, S., 2003, AJ, 125, 742

Gascoigne, S. C. B., Norris, John, Bessell, M. S., & Hyland, A. R. 1976, ApJ, 209, 25

Girardi, L., Chiosi, C., Bertelli, G., & Bressan, A. 1995, A&A, 298, 87

Girardi, L., Bressan, A., Bertelli, G., & Chiosi, C. 2000, A&AS, 141, 371

Girardi, L., Bressan, A., Bertelli, G., & Chiosi, C. 2000, A&AS, 141, 371

Lejeune Th., Cuisinier, F., Buser, R., 1997, A&ASS, 125, 229 Visvanathan, N.

Hodge, P. W. 1983, ApJ, 264, 470

Maraston C. 1998, MNRAS, 300, 872

Maraston, C., Kissler-Patig, M., Brodie, J. P., Barmby, P., Huchra, J. P., 2001, A&A, 370, 176

Matteucci, A., Ripepi, V, Brocato, E., & Castellani, V. 2002, A&A, 387, 861

Montegriffo, P., Ferraro, F.R., Fusi Pecci, F., & Origlia, L., 1998, MNRAS, 297, 872

Moorwood, A. F. M., Cuby, G. J., & Lidman, C. 1998, The ESO Messenger, 91, 9

Nikolaev, S., & Weinberg, M. D. 2000, ApJ, 542, 804

Olsen, K. A. G., Hodge, P. W., Mateo, M., Olszewski, E. W., Schommer, R. A., Suntzeff, N. B., & Walker, A. R. 1998, MNRAS, 300, 665

Olszewski, E. W., Schommer, R. A., Suntzeff, N. B., & Harris, H. C. 1991, AJ, 101, 515

Olszewski, E. W., Suntzeff, N. B., & mateo, M. 1996, ARA&A, 34, 511

Persson, S. E., Aaronson, M., Cohen, J. G., Frogel, J. A., & Matthews, K. 1983, ApJ, 266, 105

Persson, S.E., Murphy, D. C., Krzeminski, W., Roth, M., & Rieke, M., 1998, AJ, 116, 2475

Renzini, A., & Buzzoni, A. 1986, in Spectral Evolution of Galaxies, eds. C. Chiosi and A. Renzini, (Dordrecht: Reidel), 135

Rich, R. M., Shara, M. M., & Zurek, D. 2001, AJ, 122, 842

Rieke, G. H., & Lebofsky, M. J. 1985, ApJ, 288, 618

Salaris, M., & Cassisi, S., 1996, A&A, 305, 858

Sagar, R., & Pandey, A. K. 1989, A&AS, 79, 407

Santos, J. F. C., Jr., & Frogel, J. A. 1997, ApJ, 479, 764

Schlegel, D. J., Finkbeiner, D. P., & Davis, M. 1998, ApJ, 500, 525

Searle, L., Wilkinson, A., & Bagnuolo, W. G. 1980, ApJ, 239, 803

Testa, V., Ferraro, F.R., Fusi Pecci, F., Chieffi, A., Straniero, O., & Limongi, M., 1999, AJ, 118, 2839

van den Berg, S. 1998, PASP, 110, 1377

Vallenari, A., Aparicio, A., Fagotto, F., Chiosi, C. 1994, A&A, 284, 424

Yi, S., Demarque, P., Kim, Y., Lee, Y., Ree, C. H., Lejeune, T., Barnes, S. 2001, ApJS, 136, 417

Table 1. Main parameters of the target clusters.

cluster	α	δ	s	[Fe/H]	E(B-V)
NGC 1987	05:27:17	-70:44.1	35	–1.00	0.12
NGC 2108	05:43:56	-69:10.8	36	–1.20	0.18
NGC 2190	06:01:02	-74:43.5	36	–0.12	0.10
NGC 2209	06:08:34	-73:50.5	35	–1.20	0.07
NGC 2231	06:20:44	-67:31.1	37	–0.67	0.08
NGC 2249	06:25:49	-68:55.2	34	–0.12	0.10

Note. —
s-parameter from Elson & Fall (1985) and Girardi et al. (1995). Metallicity and reddening from Corsi et al. (1994) and F95 compilations. For NGC 2231 not included in Corsi et al. (1994) and F95 sample, metallicity is from Olszewski et al. (1991) and reddening from Persson et al. (1983).

Table 2. Photometry of the target clusters

Id	X	Y	J	σ(J)	H	σ(H)	K	σ(K)
NGC 1987								
1	740.819	851.305	9.819	0.011	9.558	0.007	9.519	0.007
2	501.969	368.297	12.102	0.007	10.933	0.014	10.222	0.014
3	363.867	652.862	12.146	0.002	11.001	0.012	10.341	0.012
4	491.525	460.867	12.008	0.005	11.088	0.019	10.768	0.019
5	321.522	563.854	12.031	0.007	11.098	0.011	10.788	0.011
6	746.735	480.059	12.540	0.006	11.552	0.020	11.030	0.020
7	483.386	461.947	12.497	0.009	11.611	0.022	11.275	0.022
8	909.377	911.159	12.588	0.003	11.641	0.015	11.365	0.015
9	597.747	432.049	12.659	0.006	11.741	0.017	11.426	0.017
10	390.194	379.146	13.137	0.007	12.202	0.017	11.905	0.017

Table 3. Star counts and bolometric luminosities[a].

cluster	N_{AGB}	N_{RGB}	N_{He-C}	L^{bol}_{AGB}	L^{bol}_{RGB}	L^{bol}_{He-C}
cluster population[b]						
NGC 1987	6	42	322	3.65	0.92	2.05
NGC 2108	3	40	231	2.72	1.11	1.38
NGC 2190	2	28	174	0.95	0.94	0.89
NGC 2209	3	24	160	1.53	0.61	0.81
NGC 2231	1	36	114	0.46	0.71	0.59
NGC 2249	1	9	98	0.32	0.16	0.51
field population[c]						
NGC 1987	3	90	222	0.68	2.83	1.26
NGC 2108	2	63	124	0.82	1.94	0.68
NGC 2190	0	7	18	0.00	0.17	0.11
NGC 2209	0	12	34	0.00	0.28	0.20
NGC 2231	0	13	21	0.00	0.33	0.14
NGC 2249	0	11	29	0.00	0.45	0.17

Note. —

[a] Star counts are corrected for incompleteness (see Section 4.1). Bolometric luminosities are in units of 10^4 $L_\odot$.

[b] The cluster population is de-contaminated by the field one.

[c] The field population has been normalized to the ≈ 7 arcmin^2 area, as sampled by the cluster population (see Section 3 for details).

Table 4. Age determinations for the target clusters.

cluster	s^a	s–age^b	s–age^c	TO–age ^{d}	Reference^e
NGC 1987	35	653	620	479	Girardi et al. (1995)
NGC 2108	36	783	734	525	Girardi et al. (1995)
NGC 2190	36	783	734	813	Girardi et al. (1995)
NGC 2209	35	653	620	800	Gascoigne et al. (1976)
				700	Hodge (1983)
				910	Girardi et al. (1995)
NGC 2231	37	940	869	1200	Hodge (1983)
NGC 2249	34	544	524	550^f	Vallenari et al. (1994)
				300^g	Vallenari et al. (1994)

Note. —
(^{a}) s-parameter from Elson & Fall (1985) and Girardi et al. (1995).
(^{b}) Age in Myr, according to the calibration by EF88: $log\ t = 6.05 + 0.079 \times s$.
(^{c}) Age in Myr, according to the calibration by Girardi et al. (1995): $log\ t = 6.227 + 0.0733 \times s$.
(^{d}) TO age in Myr.
(^{e}) Reference for the TO-age determination.
(^{f}) TO-age from models with *overshooting* (Vallenari et al. 1994).
(^{g}) TO-age from models with *no-overshooting* (Vallenari et al. 1994).

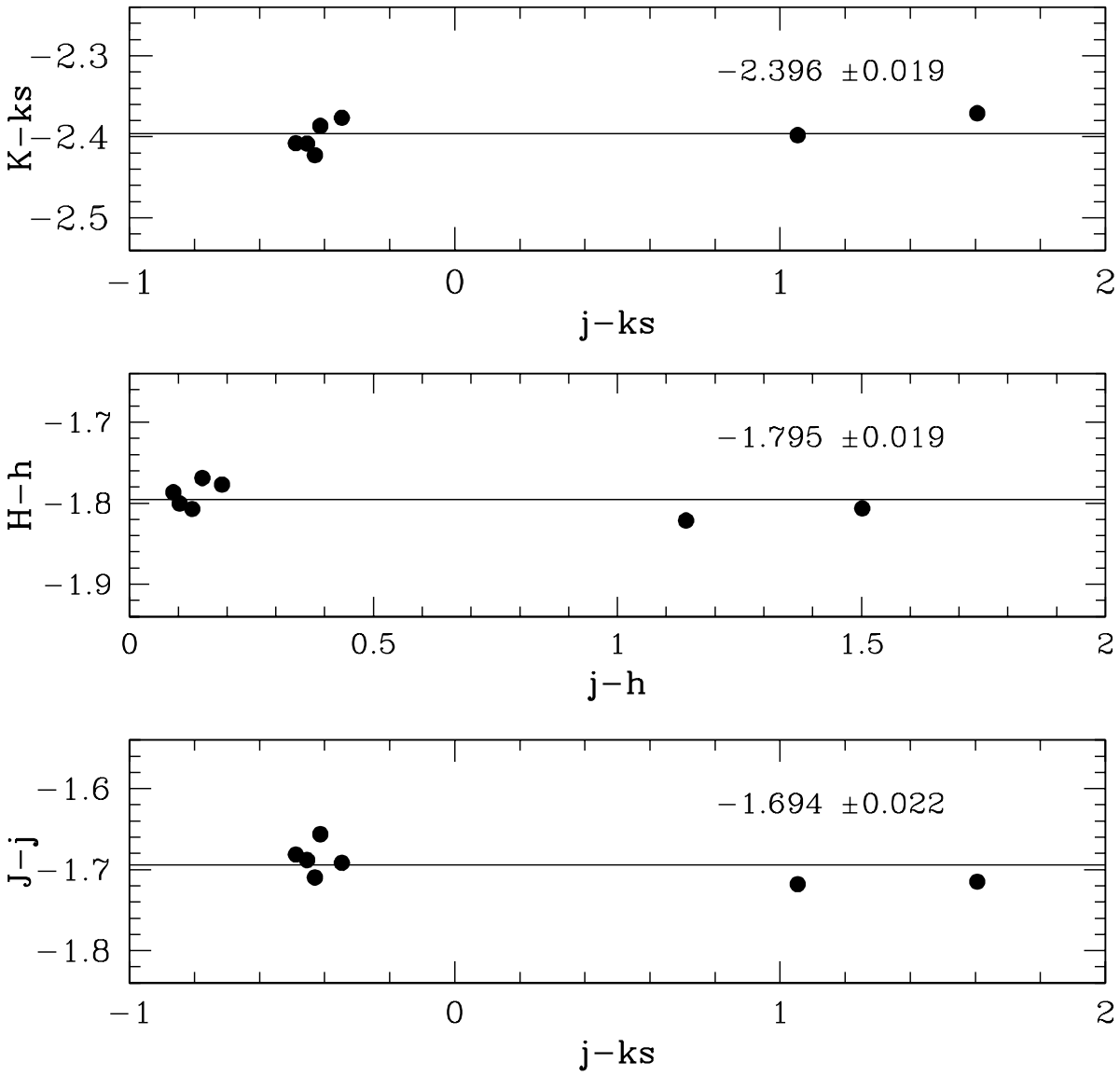

Fig. 1.— Photometric calibration. j, h, k_s are the instrumental aperture magnitudes normalized at $t_{exp} = 1sec$ and J,H,K are the corresponding calibrated magnitudes from the list of Persson et al. (1998).

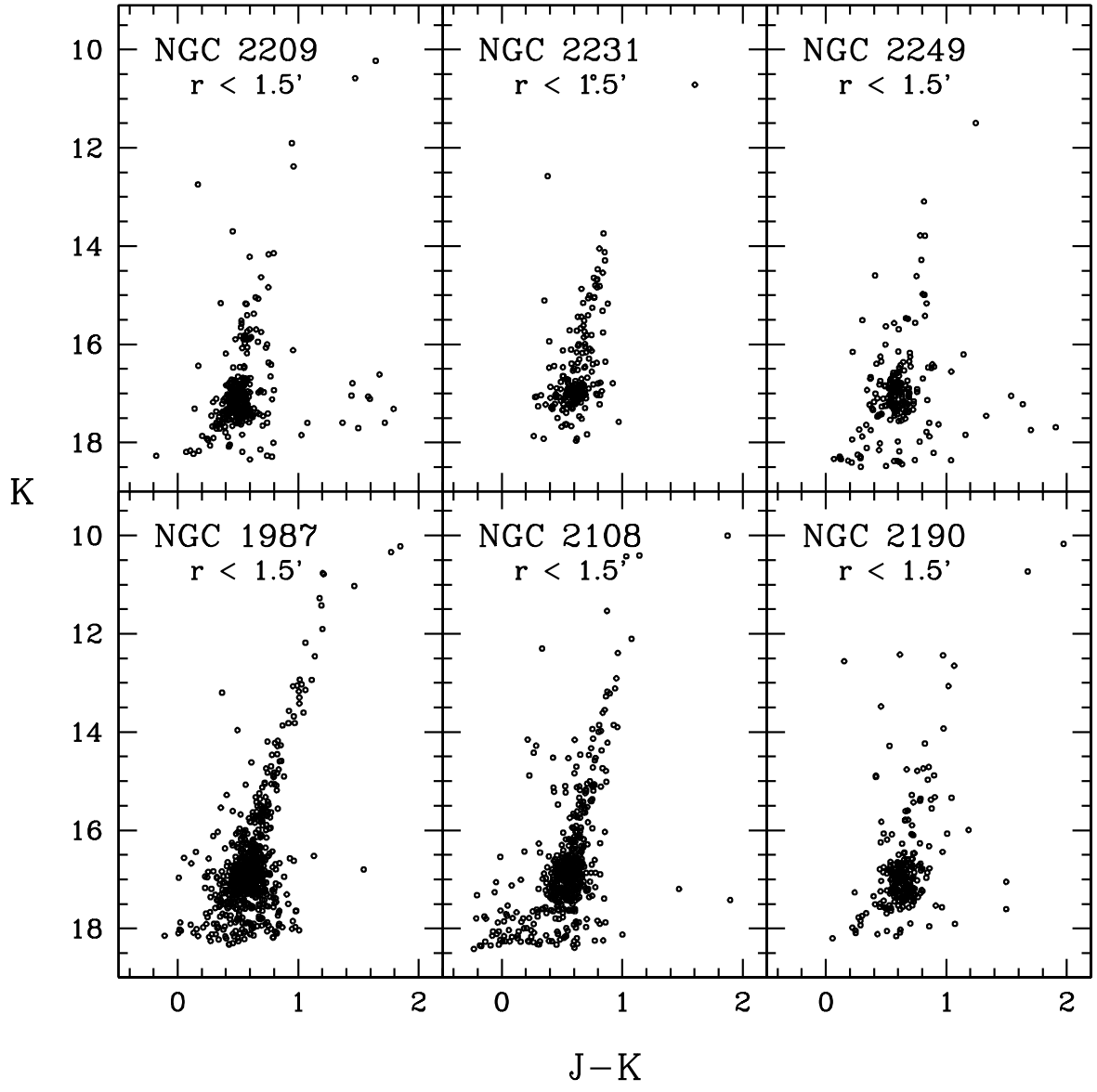

Fig. 2.— Observed (K, J−K) CMDs of the six observed LMC clusters. Only stars at $r < 1.5'$ from the cluster center are plotted, sampling a total area of $\approx$ 7 arcmin^2.

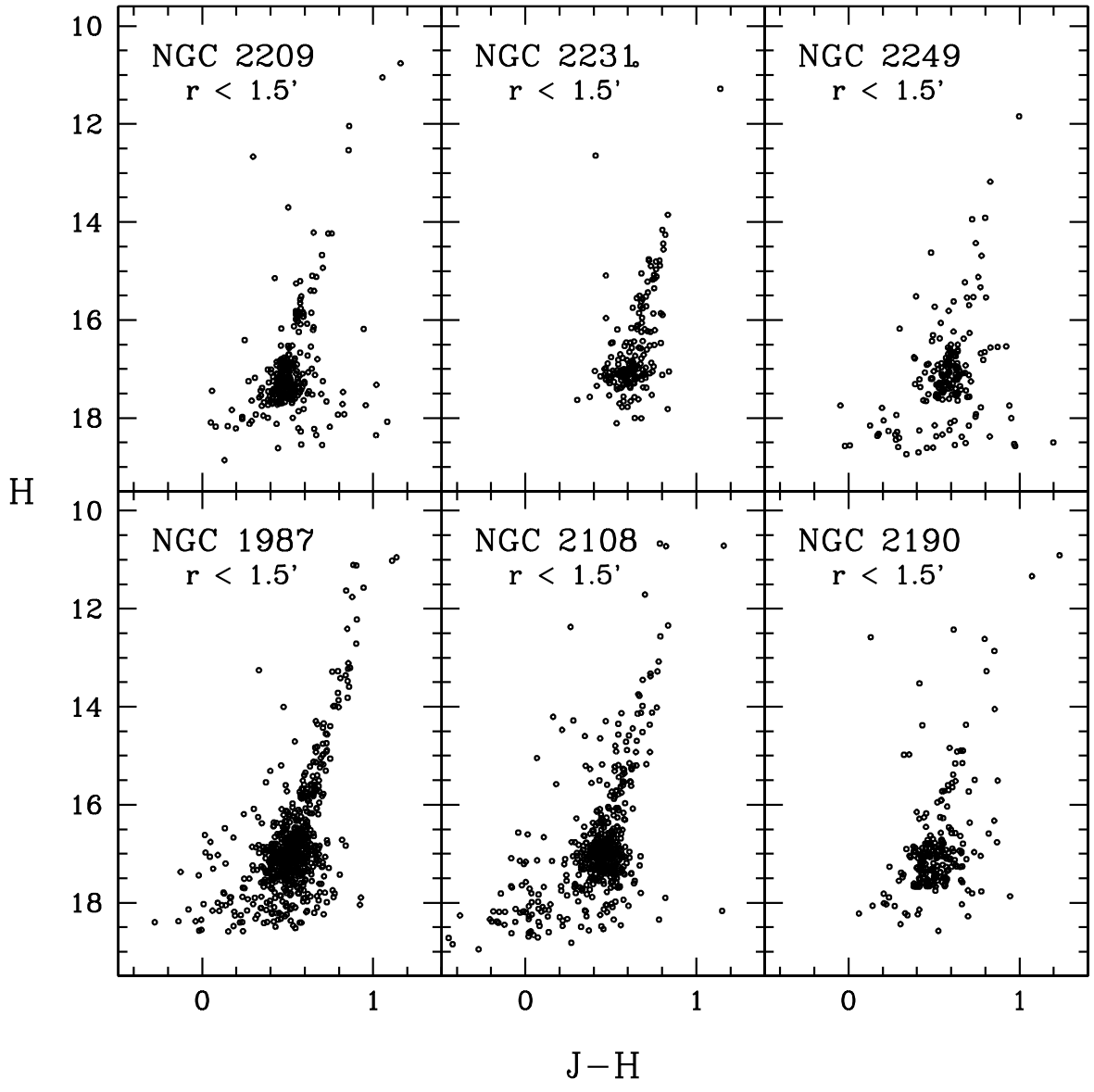

Fig. 3.— As in figure 2 but in the $(H, J - H)$ plane.

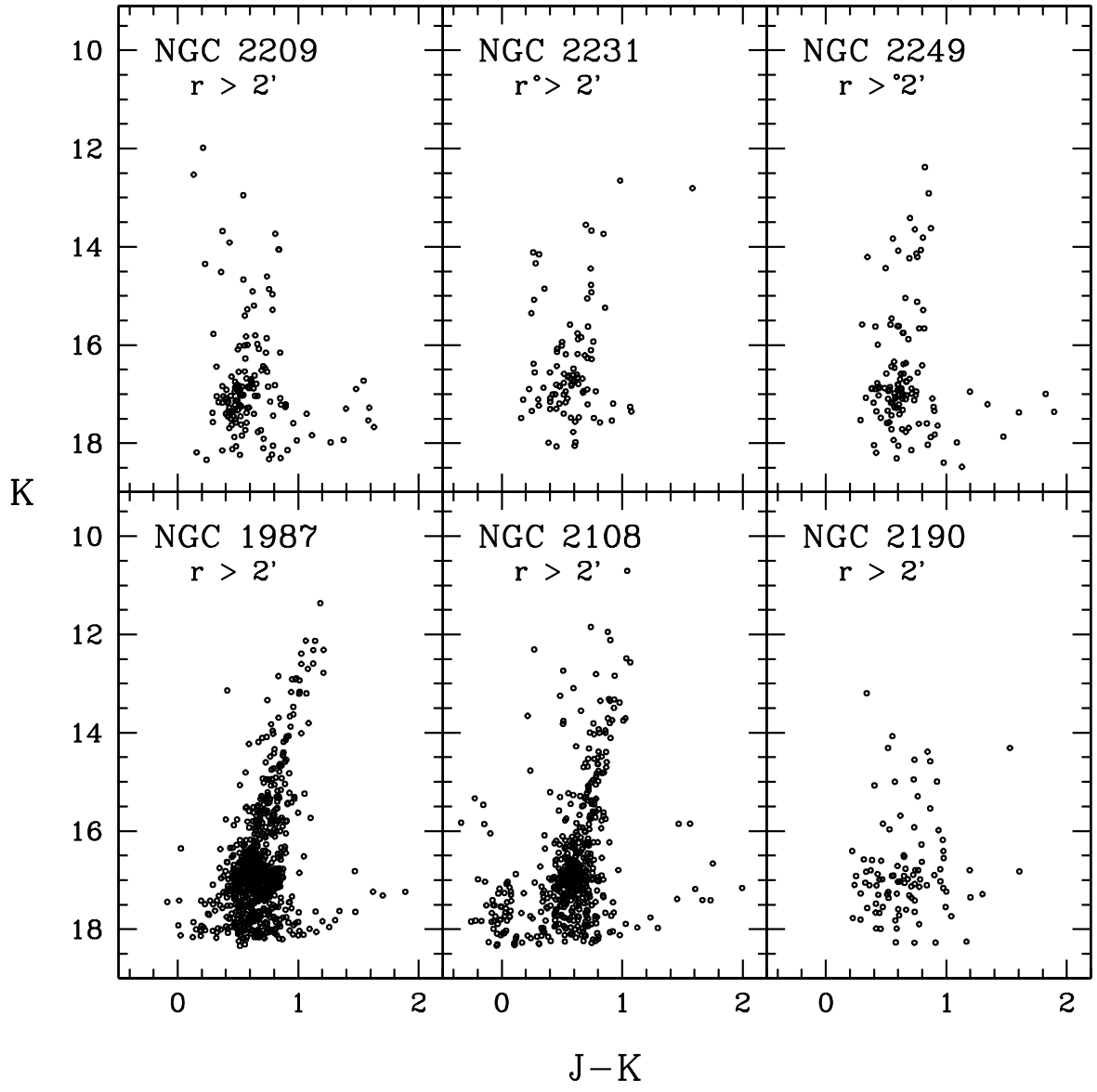

Fig. 4.— Observed (K, J − K) CMDs of the outermost (r >2') regions for the six observed LMC clusters. These CMDs are representative of the field population and sample an area of ≈ 13 arcmin^2.

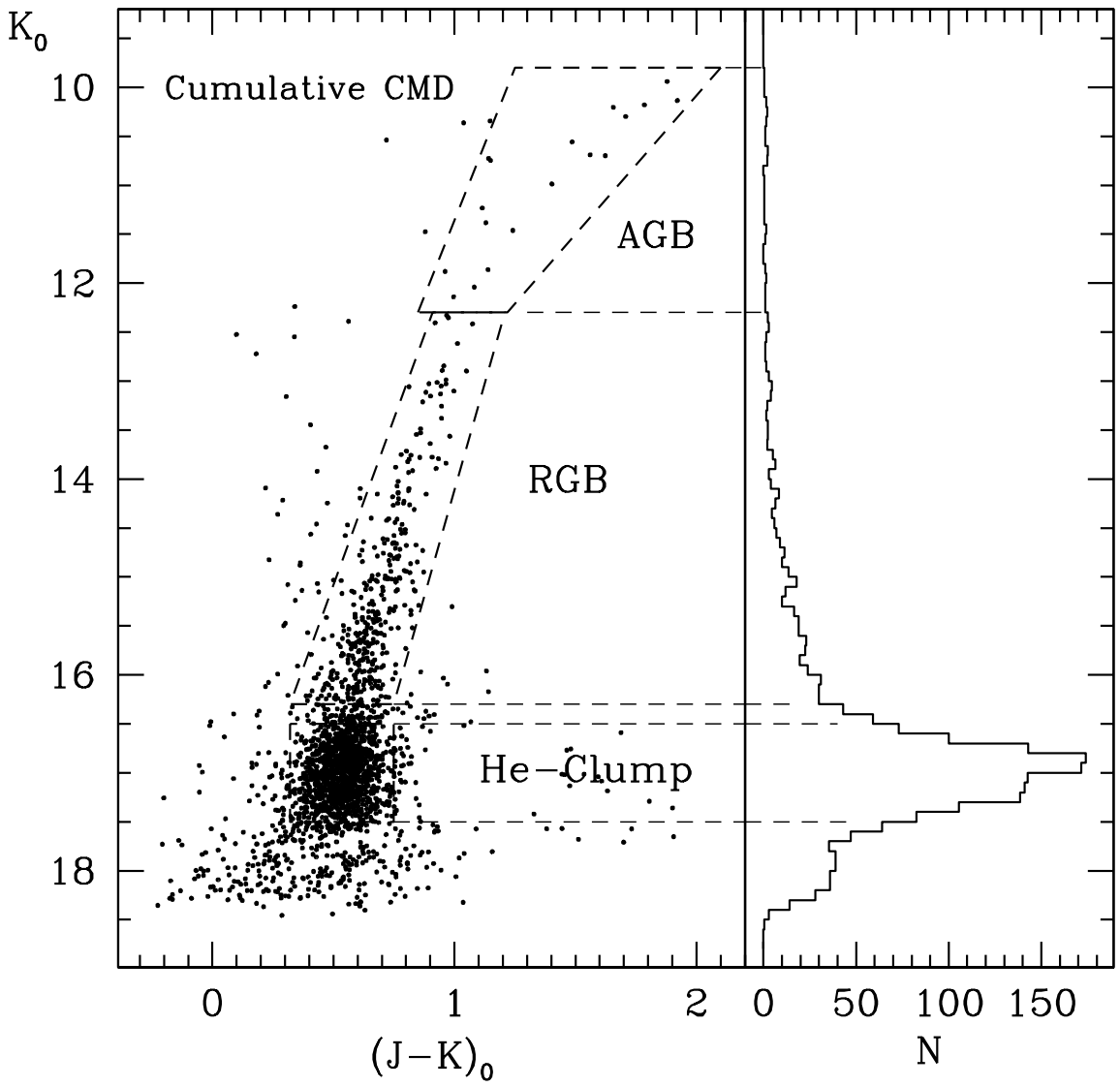

Fig. 5.— Cumulative $K_0, (J-K)_0$ de-reddened CMD (left panel) for the six observed LMC clusters. The sketched regions show schematically the AGB, the upper RGB and red He-clump loci. The corresponding differential luminosity function is also shown for clarity (right panel).

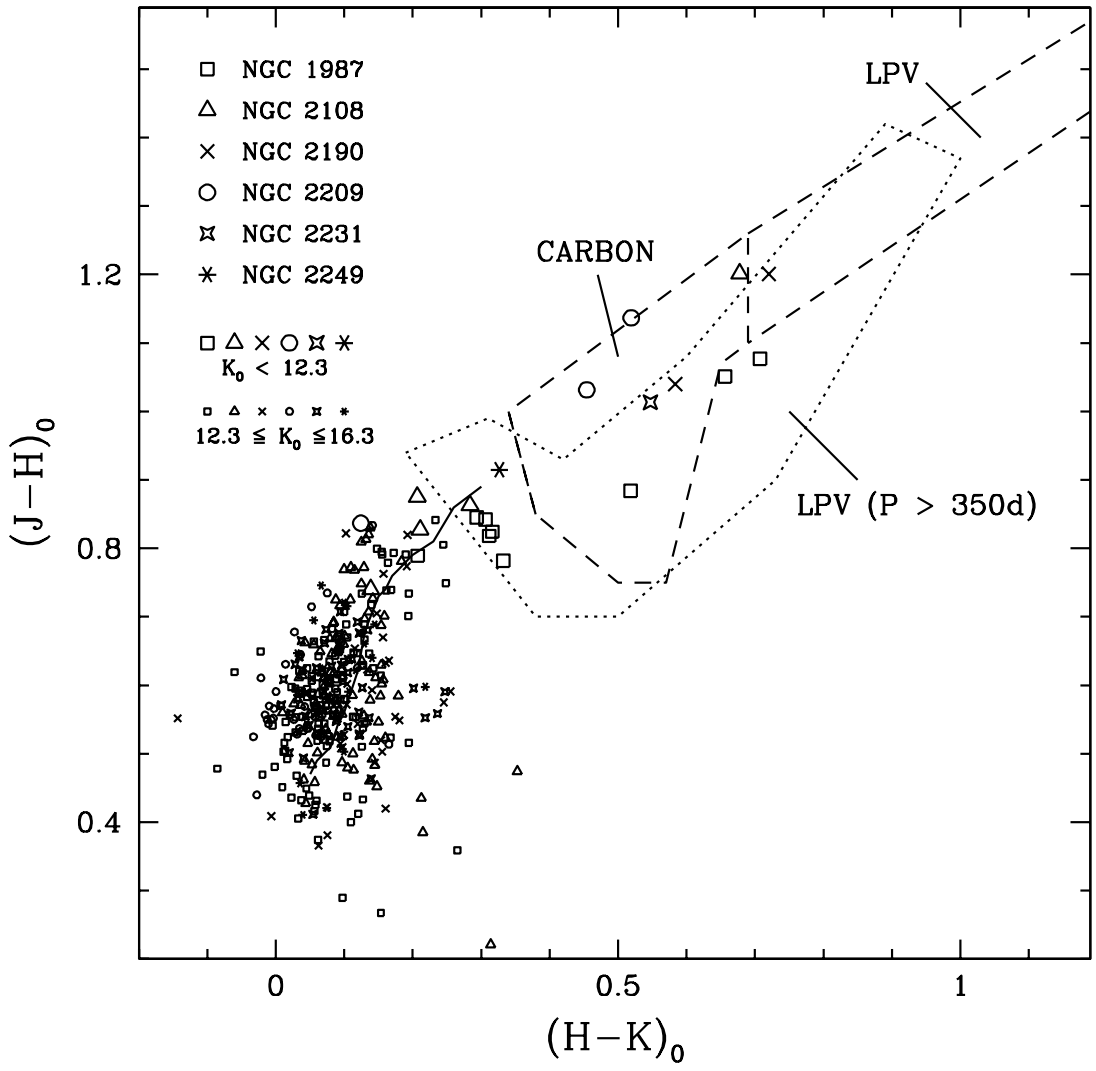

Fig. 6.— Cumulative $(J-H)_0, (H-K)_0$ de-reddened color-color diagram for the six observed LMC clusters. Only the AGB and RGB stars, as classified accordingly to the *selection boxes* defined in Section 3 and sketched in Figure 5, are considered. Small symbols are stars with $16.3 \leq K_0 \leq 12.3$ while big symbols represents stars brighter than the RGB Tip (at $K_0 < 12.3$), and they are, most likely, AGB variables. Solid line indicates the mean locus for K giants (Frogel et al. 1978). Dotted and dashed lines delimit the CMD region occupied by field LPV and Carbon stars, solid line the mean locus of field K giants (Bessel & Brett 1988, F95 and references therein).

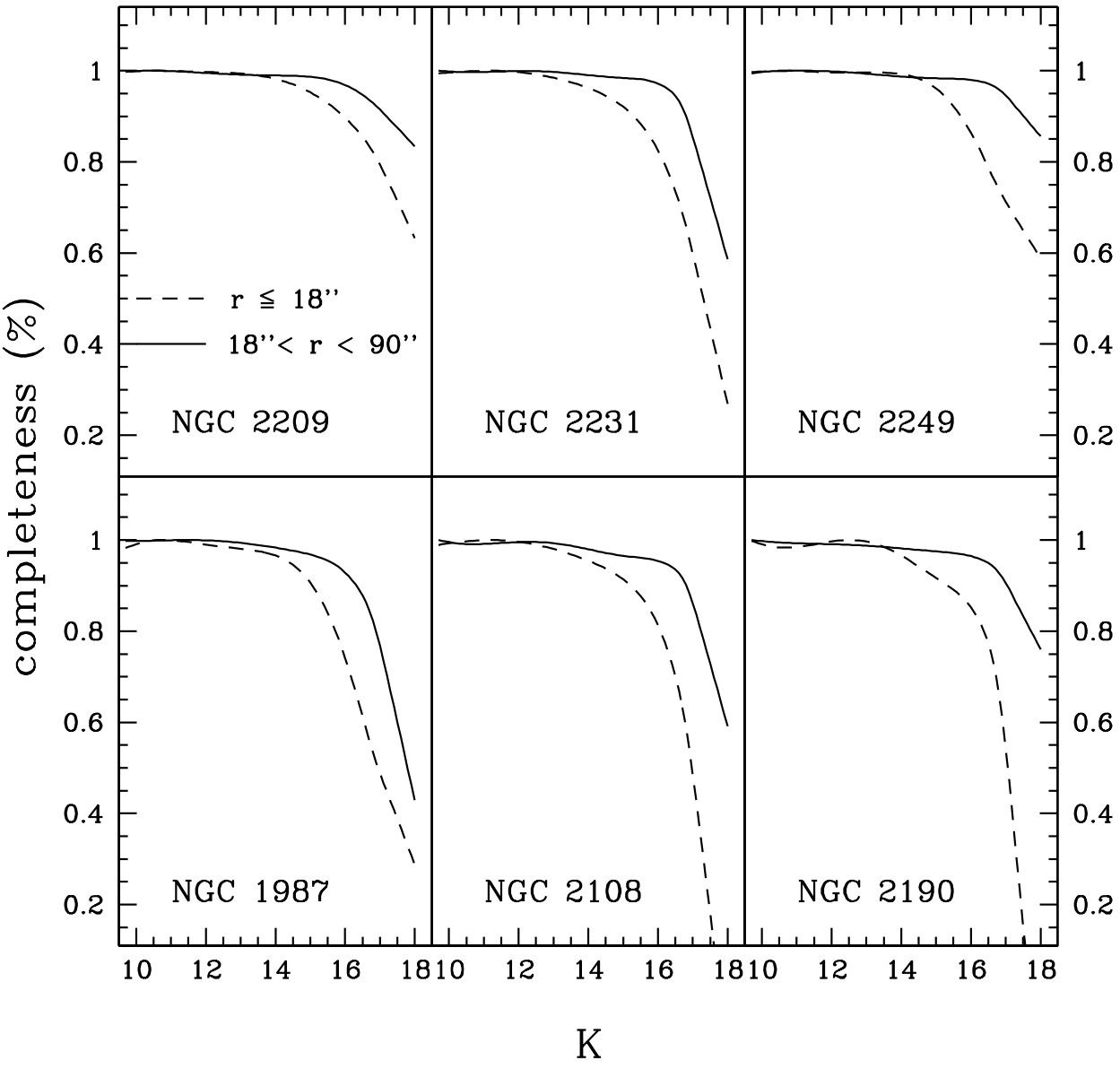

Fig. 7.— Completeness curves. Dashed lines: $r \leq 18''$, solid lines: $18'' < r < 90''$ (see Section 4.1).

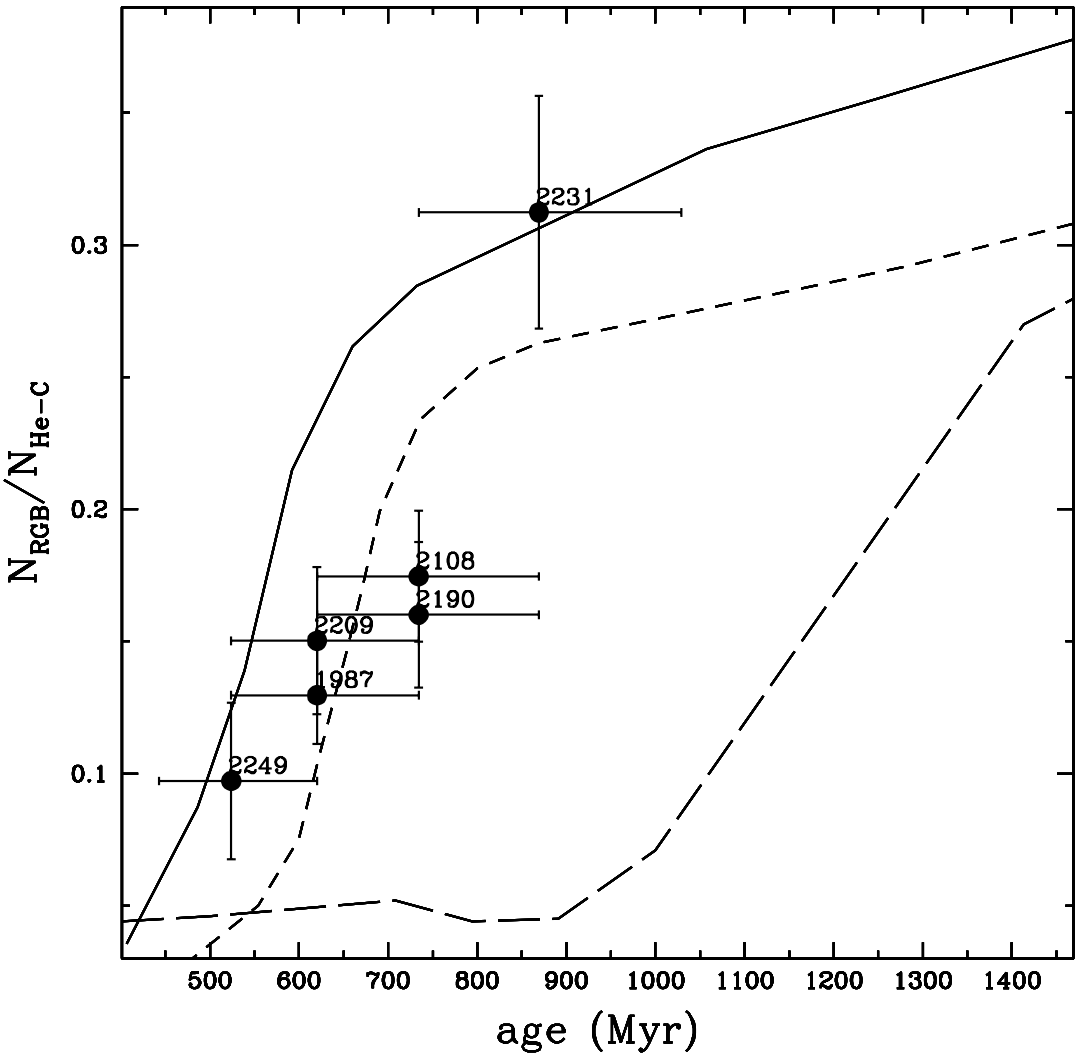

Fig. 8.— Ratio between the number of the bright RGB and He-clump stars as a function of age for the six observed clusters, Stars belonging to the two populations are selected accordingly to the *selection boxes* defined in Section 5 and shown in Figure 5. Short-dashed and solid lines represent *canonical* models at two different metallicities, namely [Z/H]=–0.33 and –1.35, respectively, (see Maraston 1998, and Section 4), while long-dashed line is the result by using *overshooting* tracks at [Z/H]=–0.4 from Girardi et al. (2000).

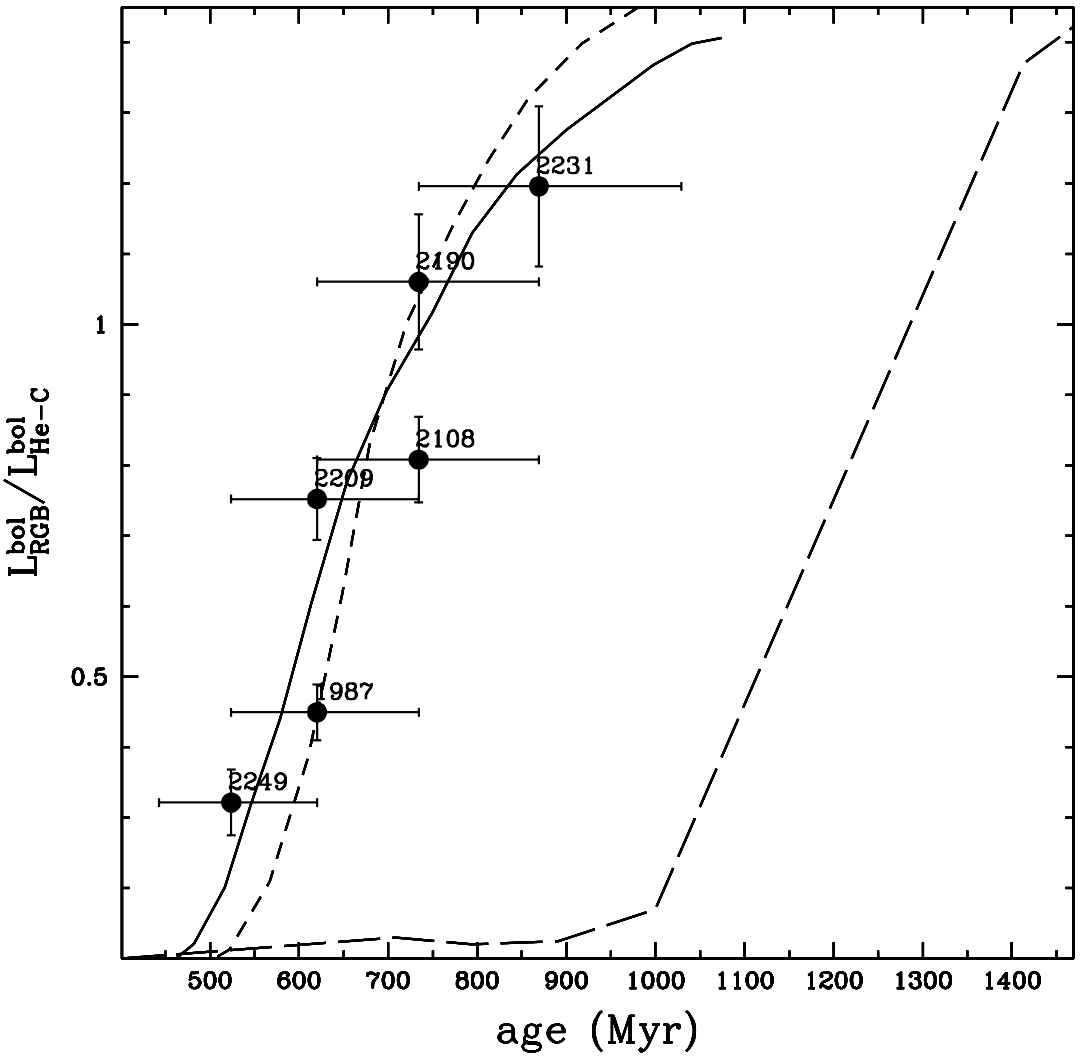

Fig. 9.— Ratio between the bolometric luminosity of the bright RGB and He-clump stars as a function of age for the six observed clusters. Star belonging to the two populations are selected accordingly to the *selection boxes* defined in Section 5 and shown in Figure 5. Short-dashed and solid lines represent *canonical* models at two different metallicities, namely [Z/H]=–0.33 and –1.35, respectively (see Maraston 1998, and Section 4), while long-dashed line is the result by using *overshooting* tracks at [Z/H]=–0.4 from Girardi et al. (2000).